II International Conference on Particle-based Methods - Fundamentals and Applications
PARTICLES 2011
E. Oñate and D.R.J. Owen (Eds)

INCIPIENT SEDIMENT TRANSPORT FOR NON-COHESIVE LANDFORMS BY THE DISCRETE ELEMENT METHOD (DEM)

R. Bravo*, P. Ortiz* and J.L. Pérez–Aparicio†

*University of Granada
Escuela de Caminos
Campus de Fuentenueva, 18071 Granada, Spain
e-mail: rbravo@ugr.es, portiz@ugr.es

†Department of Continuum Mechanics and Theory of Structures
Universidad Politécnica de Valencia
Camino de Vera s/n. 46022. Valencia, Spain
e-mail: jopeap@upvnet.upv.es

Key words: Granular Materials, DEM, FEM, Contact Problems

Abstract. The determination of the shear stress at which a sediment grain of a given size and density starts to move has been treated with theoretical, experimental and numerical procedures by many authors. The seminal contribution of Shields [7] addresses a relationship for the non-dimensional critical shear stress in terms of the friction Reynolds number for a single particle in a flat bed.

This work focusses on the incipient transport of particles for bedforms. The proposed numerical approach to the problem integrates the Discrete Element Method (DEM) [9] with a continuous finite element approximation. The DEM simulates the motion of the landform, defined as an aggregate of rigid discs that interact by contact and friction. The continuous finite element approach predicts the boundary shear stress field coming from the fluid flow over the bed (for basic formulation, see [4] and reference therein). Both methods are coupled through the flow-particle force transmission using drag coefficients. While for single particles (or very simple sets of particles) incipient motion (and consequently, the threshold stress) is clearly defined, for complex forms the use of the concept of incipient transport becomes necessary, and critical shear stress is established in terms of a threshold sediment flux over the bed surface.

We present a series of numerical experiments for single particles, showing good agreement with Shields curve for the whole range of Reynolds number. In this communication we show some of these results, in compare with the basic Shields curves for flat bed and single grains.

1 Introduction

The mechanics of sediment transport is the keystone of many fields. Many authors have carried out experimental studies to analyze, measure and predict the sediment transport under many conditions since there is not a general analytical formulation or a numerical approach that analyzes the sediment transport accurately. This paper establishes a new numerical approach in the analysis of the motion treshold of granular particles, simulating the initiation of sediment transport in the interface between fluid and sediment through the numerical coupling of the Discrete Element Method (DEM) for particles and the Finite Element Method for fluid.

Shields was the first reference to define a curve that defines the initiation of motion relating and the Reynold's number. This curve was based in dimensional considerations and experimental data, therefore it was not able to define the motion of the individual particles. The new approach considers the real behaviour of granular materials simulating the entraiment kinematics and particle interactions through contact. The Discrete Element Method is a powerful tool to model the geometry and interactions since its formulation is based in the balance momentum equation plus the additional restrictions with contact. The flow interaction is inserted in model using the lift and drag forces from [3]. The proposed work obtains the initiation of motion for situations in which shield's curve is not able to provide reliable data.

2 Analytical theory

The available analytical theories [3], [8] are based in the analysis of the motion of a single particle over a sediment bed. This situation is depicted in Fig. 1 where the motion of the underneath particles is restricted, therefore it represents the worst situation. If the scheme from Fig. 1 is repeated periodically, then it represents a sediment bed Fig. 2.

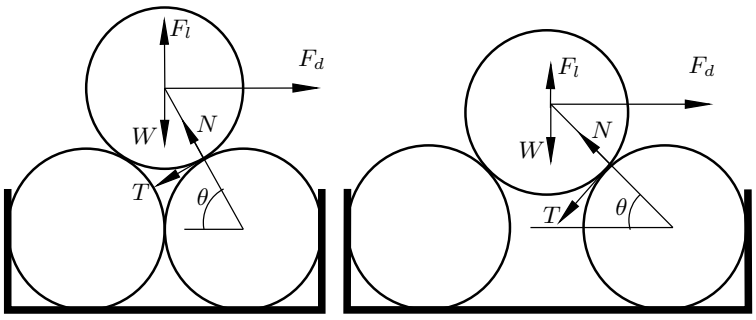

Figure 1: Single particle over a sedimentary bed

The balance of forces of Fig. 1 allows to obtain the combination of drag F_d and lift F_l forces for any friction angle ϕ and compacity angle θ that initiates the motion of a single

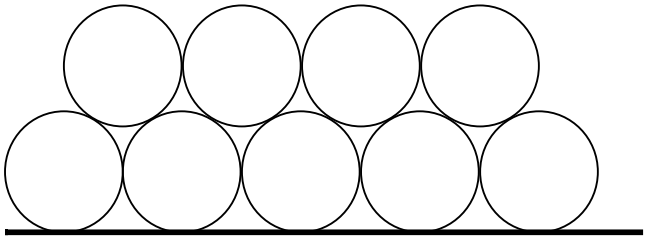

Figure 2: Sedimentary bed, obtained as a periodic repetition of the scheme depicted in Fig. 1

particle. Solving these equations it is possible to obtain the normal N, tangential forces T and the relation between F_d and F_l for the initiation of motion.

$$\begin{array}{c} F_l + F_d \tan\theta = W; T = F_d \sin\theta + (F_l - W)\cos\theta; \\ N = F_d \tan\theta(1 - \sin\theta) + (W - F_l)\sin\theta \end{array} \tag{1}$$

This equilibrium equation allows to obtain the relation between $u^\star$ and the Reynolds number $R^\star$ that forces the for two situations

2.1 Small Reynolds Numbers

In this section we briefly describe the derivation of the drag for drag F_d and lift forces F_l as function of shear frictional velocity $u^\star$ and therefore a relationship between shear stress $\tau = u^{\star 2}\rho_f$ and reynolds number $Re^\star$ for a single particle of diameter d. These expressions inserted in Eqs. 1 provide the condition for the initiation of motion as function of $u^\star$. For low Reynolds number $R^\star < 30$, the velocity distribution around the particle is linear. Therefore the mean flow velocity is defined as:

$$V_f = \frac{u^{\star\,2}}{2\nu} d; \text{ while } F_d \text{ and } F_l \text{ are given by: } F_d = \frac{3}{2}\pi\tau d^2; \; F_l = \frac{1}{2}\frac{u^\star d}{\nu}\tau d^2 \tag{2}$$

where ν is the viscosity, ρ_s and ρ_f are the densities of the solid and fluid respectively. Combining Eqs. 1 and 2 provides a relation between $u^\star$ and the reynolds number:

$$\frac{\tau}{(\rho_s - \rho_f)gd} = \frac{\pi/6}{3\pi\tan\theta + \frac{1}{2}\frac{u^\star d}{\nu}} \tag{3}$$

2.2 Large Reynolds Numbers

For large Reynolds number $R^\star \geq 30$ the velocity distribution around the particle is logarithmic and is given by the following expression:

$$\frac{u}{u^\star} = 2.5 \log\frac{z}{z_0} \quad \frac{\partial u}{\partial z} = 2.5 u^\star \frac{1}{z} \tag{4}$$

Using these last two results the expressions for the drag F_d and lift F_l forces are:

$$F_d = \tfrac{1}{8} C_d \pi \tfrac{V_f}{u^\star}^2 \tau d^2;\ F_l = \frac{V_f}{u^\star}\left(\frac{\partial u}{\partial z}\frac{d}{u^\star}\right)^{0.5}\left(\frac{u^\star d}{\nu}\right)^{0.5}\tau d^2; \\ C_d = \tfrac{24\nu}{d}\left[1 + 0.15\left(\tfrac{V_f d}{\nu}\right)^{0.687}\right] \tag{5}$$

In similar way as in the previous subsection, it is possible to define an adimensional relation that provides $u^\star$ as function of $R^\star$.

$$\frac{\tau}{(\rho_s - \rho_f) g d} = \frac{\pi/6}{\frac{V_f}{u^\star}\left(\frac{\frac{\partial u}{\partial z}}{u^\star}\right)^{0.5}\left(\frac{u^\star d}{\nu}\right)^{0.5} + \frac{\pi}{8} C_d \left(\frac{V_f}{u^\star}\right)^2} \tag{6}$$

3 DDA GENERIC FORMULATION

3.1 Introduction

From the pioneering work of [6] on the Discrete Element Method (DEM), [5] extended this method to another one called Discrete Deformation Analysis (DDA) for the analysis and modeling of the mechanical response of rock assemblies. The reason for DDA's reliability is that it reflects the mechanics of the phenomenon associated with the movement of the particles; beyond the exact representation of basic material and geometrical properties, it simulates mechanical interactions explicitly.

3.2 Governing equations

This subsection describes the problem and the corresponding governing equations including the contact equation in DDA based on Hamiltonian mechanics.

3.2.1 Hamiltonian description of motion

Hamiltonian mechanics permit to obtain the equations of motion for every point of multiple particles that interact by contact. The particles are still considered a continuum. Each point x, y in each particle i is characterized by its position $\boldsymbol{Q}^i(x,y,t)$ and its linear momentum $\boldsymbol{P}^i(x,y,t)$. The Hamiltonian function $H\big[\boldsymbol{Q}(x,y,t), \boldsymbol{P}(x,y,t)\big]$ defines the total energy of the set of particles, that is assumed to be separable in kinetic $K(\boldsymbol{P}(x,y,t))$ and potential $\Pi(\boldsymbol{Q}(x,y,t))$ energies:

$$H\big[\boldsymbol{Q}(x,y,t), \boldsymbol{P}(x,y,t)\big] = \sum_{i=1}^{n_{bd}} \big[K\big(\boldsymbol{P}^i(x,y,t)\big) + \Pi\big(\boldsymbol{Q}^i(x,y,t)\big)\big]$$

$$K\big(\boldsymbol{P}^i(x,y,t)\big) = \frac{1}{2}\int_{\Omega^i} \frac{\boldsymbol{P}^i(x,y,t)^2}{\rho_s}\,\mathrm{d}\Omega; \Pi\big(\boldsymbol{Q}^i(x,y,t)\big) = \int_{\Omega^i} \boldsymbol{Q}^i(x,y,t)^T\ \boldsymbol{f}\big(\boldsymbol{Q}^i(x,y,t)\big)\,\mathrm{d}\Omega \tag{7}$$

where n_{bd} is the total number of particles and Ω^i the particle domain. The kinetic and potential energies are real scalar functions and ρ_s is the particle density, assumed constant. In this work, the potential energy Π is related with forces external and due to contact, generically represented in Eq. 7 by $\boldsymbol{f}\big(\boldsymbol{Q}^i(x,y,t)\big)$, [6]. The motion of particle i is then governed by the Hamiltonian canonical equations [2]:

$$\begin{aligned} \dot{\boldsymbol{Q}}^i(x,y,t) &= \frac{\partial H[\boldsymbol{Q}(x,y,t),\boldsymbol{P}(x,y,t)]}{\partial \boldsymbol{P}^i} = \int_{\Omega^i} \frac{\boldsymbol{P}^i(x,y,t)}{\rho_s}\,\mathrm{d}\Omega \\ \dot{\boldsymbol{P}}^i(x,y,t) &= -\frac{\partial H[\boldsymbol{Q}(x,y,t),\boldsymbol{P}(x,y,t)]}{\partial \boldsymbol{Q}^i} = -\nabla\Pi\big(\boldsymbol{Q}^i(x,y,t)\big) \end{aligned} \tag{8}$$

and where the supra dot indicates derivative with respect to time.

3.2.2 Discretization

Often it is not possible to find an analytical solution of the previous equations; we have to obtain an approximated solution through the discretization of variables $\boldsymbol{Q}$, $\boldsymbol{P}$ from Eqs. 8. For every point x, y of particle i, these variables are interpolated from values defined at several points called nodes.

$$\boldsymbol{Q}^i(x,y,t) = \boldsymbol{N}(x,y)\ \boldsymbol{q}^i(t)\ ; \qquad \boldsymbol{P}^i(x,y,t) = \boldsymbol{N}(x,y)\ \boldsymbol{p}^i(t) \tag{9}$$

where $\boldsymbol{N}$ is the shape function associated to the node, usually defined at the center of gravity x^i, y^i. These shape function matrix contain the interpolating polynomials, see an example in subsection 5. Usually in DDA a single node is defined at the gravity center and consequently the variables at this node are the unknowns of the problem. These nodal displacements $\boldsymbol{q}^i$ and linear momenta $\boldsymbol{p}^i$ for all particles nodes at a given time are grouped in the vectors $\boldsymbol{q}(t)$, $\boldsymbol{p}(t)$.

For each particle i, the discretization Eqs. 9 combined with Eqs. 8 produce the system of equations:

$$\dot{\boldsymbol{q}}^i = \boldsymbol{M}_i^{-1}\ \boldsymbol{p}^i\ ; \qquad \dot{\boldsymbol{p}}^i = -\boldsymbol{N}^T\ \nabla\Pi\big(\boldsymbol{N}\boldsymbol{q}^i\big) = \boldsymbol{f}_c^{i\prime} + \boldsymbol{f}_{ext}^{i\prime} \tag{10}$$

where $\boldsymbol{M}_i^{-1}$ is the inverse of a diagonal mass matrix, with entries $\boldsymbol{M}_i = \int_{\Omega^i} \boldsymbol{N}^T\ \rho_s\ \boldsymbol{N}\ \mathrm{d}\Omega$ and $\dot{\boldsymbol{p}}^i \equiv \boldsymbol{f}_c^{i\prime} + \boldsymbol{f}_{ext}^{i\prime}$ is the discrete counterpart for Newton's second law (contact forces $\boldsymbol{f}_c^{i\prime}$ plus the discrete external $\boldsymbol{f}_{ext}^{i\prime}$). Finally, Eqs. 10 are integrated in time using the energy consistent formulation of [1].

4 DESCRIPTION OF CONTACT

Consider two rigid particles i, k the domains of which are defined by Ω^i, Ω^k and with boundaries $\Gamma^i = \partial\Omega^i$, $\Gamma^k = \partial\Omega^k$ (Fig. 3). These particles interact through contact and it is possible to obtain the magnitude that defines the separation between particles by the gap function:

$$g_N^{ik}(\boldsymbol{X}) \;\leftrightarrow\; g_N^{ki}(\boldsymbol{Y}(\boldsymbol{X})) = \left[\boldsymbol{q}^i(\boldsymbol{X}) - \boldsymbol{q}^k(\boldsymbol{Y}(\boldsymbol{X}))\right]\, \boldsymbol{R}^{ki} \tag{11}$$

The variables $\boldsymbol{q}^i(\boldsymbol{X})$ and $\boldsymbol{q}^k(\boldsymbol{Y}(\boldsymbol{X}))$ are the positions of the closest-points $\boldsymbol{X}$, $\boldsymbol{Y}$ and $\boldsymbol{R}^{ki}$, see Fig. 3, is the normal unit vector. The gap function has to satisfy the constraint $g_N^{ik} \geq 0$ or impenetrability condition.

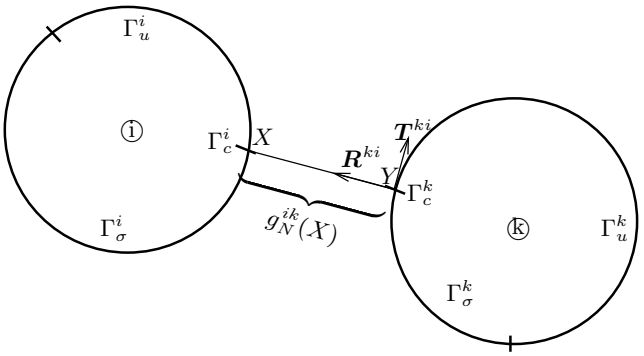

Figure 3: Contact between two particles i, k: closest point projection mapping

The interaction of two rigid rounded particles at point $\boldsymbol{X} \equiv \boldsymbol{Y}(\boldsymbol{X})$ is defined by the contact force $\boldsymbol{f}_c^{ik}$:

$$\boldsymbol{f}_c^{ik} = f_{cN}^{ik}\, \boldsymbol{R}^{ik} + f_{cT}^{ik}\, \boldsymbol{T}^{ik} \tag{12}$$

where f_{cN}^{ik}, f_{cT}^{ik} are the components of the contact force and $\boldsymbol{R}^{ik}$, $\boldsymbol{T}^{ik}$ the unit vectors in the normal and tangential directions respectively, all of them at contact point $\boldsymbol{X}$. The contact forces are formulated as $\boldsymbol{f}_{cN}^{ik} = K_N g_N^{ik}$, $\boldsymbol{f}_{cT}^{ik} = K_T g_T^{ik}$ for the Stick case and as $\boldsymbol{f}_{cN}^{ik} = K_N g_N^{ik}$, $\boldsymbol{f}_{cT}^{ik} = \mu \boldsymbol{f}_{cN}^{ik}$ for the Slip case. Physically, the penalty parameters K_N, K_T are equivalent to high stiffness elastic springs between the contact points, therefore avoiding the possibility of penetration (Fig. 4).

5 Numerical coupling

We are going to focus on the coupling of F_d and F_l in DEM considering like point forces applied in the center of gravity of each mass. Without loss of generality we consider a

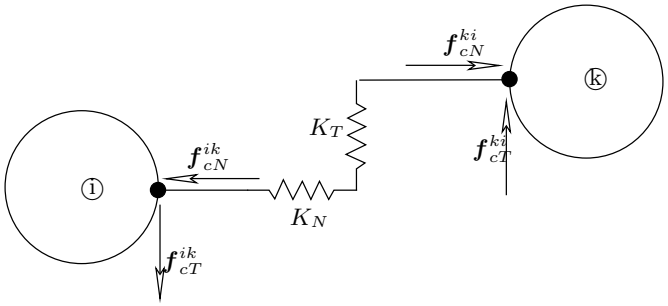

Figure 4: Contact model and penalty parameters

point force F_x, F_y applied in (x, y) and subjected to (Q_x, Q_y). Therefore the potential energy is:

$$\Pi_i = -(Q_x F_x + Q_y F_y) = -\begin{pmatrix} Q_x \\ Q_y \end{pmatrix}^t \begin{pmatrix} F_x \\ F_y \end{pmatrix} = -q_i^t \left(N_i^t \begin{pmatrix} F_x \\ F_y \end{pmatrix} \right) \tag{13}$$

Minimizing Π_i respect to q_i^t:

$$\frac{\partial \Pi_i}{\partial q_i^t} = \frac{\partial}{\partial q_i^t} q_i^t \left(N_i(x,y)^t \begin{pmatrix} F_x \\ F_y \end{pmatrix} \right) = N_i^t \begin{pmatrix} F_x \\ F_y \end{pmatrix} \rightarrow f_{ext} \tag{14}$$

Therefore, substituting the x, y components of the discrete point drag and lift forces in F_x, F_y given by the NStokes formulation in every time step and applying in gravitu center of each body, we obtain the expression for these forces in DEM.

6 Description of the coupled numerical model

6.1 Description of NStokes

Accurate prediction of sediment transport depends on a proper computation of stresses in the boundary layer. The computed stress field is obtained from the flow by means of a continuous finite element model for the incompressible Navier-Stokes equations (for details see Refs. [10] and [4]). Once stress field is calculated, values on the boundary layer are used to compute drag and lift forces by transforming shear stresses to drag and lift forces using Eqs. 2.

7 Numerical results

7.1 Shields diagram for flat surface

Analytical formulation for the initiation of sediment motion is usually based on the following dimensionless relation : $\dfrac{\tau}{(\rho_s - \rho_f) g d} = F\left(\dfrac{u^\star d}{\nu}\right)$. The famous Shields diagram [7]

was obtained fitting the previous relation to the experimental data and is depicted in Fig. 7.1.3. The numerical approach simulates accurately the micromechanics that analytical formulations cannot take into account, like the rolling or sliding between particles for several geometries and frictional materials. In order to prove the efficiency of the numerical approach, this will be applied to simulate the analytical formulation from [3] and the experimental data from Shields.

7.1.1 Numerical setup

The experimental setup is depected in Fig. 1, where the rigid lateral boundaries avoid the motion of spheres 1 and 2 while sphere 3 may slide or roll over them. This configuration is computationally attractive since it simulates a periodic boundary, see Fig. 2 that prevents the displacement of spheres 1 and 2. These particles do not roll due to the high imposed friction coefficient.

In this situation, only particle 3 interacts with fluid since it is considered that the motion is parallel to the surface. It is expected that the numerical approach fits well the analytical ones due to both have the same set up. In this simple case, sphere 3 is only affected by the fluid force using drag and lift forces F_d and F_l defined by coefficients C_d and C_l.

7.1.2 Solution procedure.

As seen in Shields diagram [7] and analytical formulations [3], several variables depend both the x and y axes, therefore we have to use an iterative procedure to obtain the solution that represents the initiation of motion. This is summarized in these steps:

- Input data: initial d, final d, increment of Δd, $\Delta u^\star$, , ν, tol.
- For every size d:
  - Start wit a given $u^\star = \Delta u^\star$
  - Compute $Re^\star$, the decide if laminar or turbulent situation is reached. Usually laminar for $Re^\star < 5$.
  - Compute drag and lift forces f_d, f_l and apply to sphere.
  - Verify initiation of motion with DDA.
    - If total displacement $<$ tol. No motion, then $u^\star = u^\star + \Delta u^\star$ and go to the second item.
    - Otherwise. Compute $\tau^\star$. $d = d + \Delta d$

After applying this procedure, the diagram depicted in Fig. 7.1.3 is obtained. It is important to remark that for $5 < Re^\star < 30$ there is a transition from laminar to turbulent flow that makes difficult that the numerical and analytical data fit wit the experimental ones.

7.1.3 Analysis results

Fig. 7.1.3 shows the numerical, analytical and experimental results for the Shields diagram. Analytical results show two limiting situations, that correspond to the initiation of motion by rolling or lifting. The experimental and numerical results fall between this situations. It is clear that the numerical model only predicts the initiation of motion by rolling since the numerical model is only able to simulate such initiation. For low $Re^\star$ the drag force F_d is linear, then the left part of the logarithmic Shield's diagram is almost planar. Real particles are not fully spherical, then the drag coefficient C_d and the friction is higher than that for a sphere and a high stress $\tau^\star$ is needed to initiate the motion. That is the reason that experimental results provides higher values than the analytical and experimental. For turbulence, the velocity distribution around particles is logarithmic, therefore the relation given by the right part of the logarithmic graph is linear.

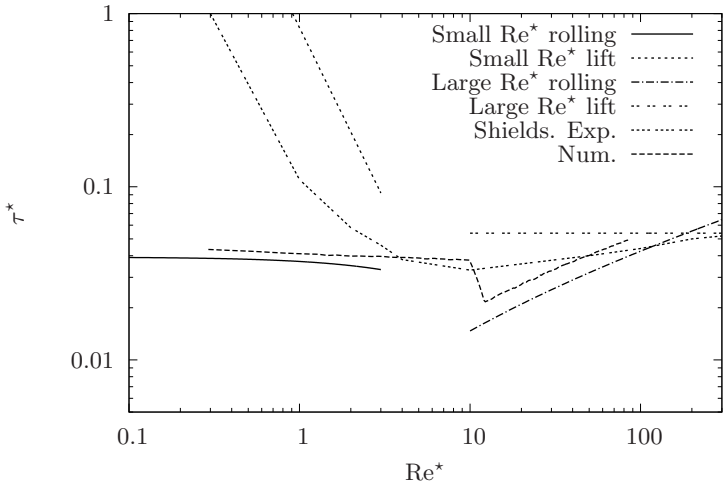

Figure 5: Shield's diagram for a single particle, experimental, analytical and numerical results

7.2 Shields diagram for inclined surfaces

This example analyses the initiation motion of the external inclined sides of a triangular shaped assembly composed by thousands of circular rigid particles of the same radius, as shown in Figs. 7.2.2. This analysis is focused in the surface particles since this is the interface between landform and fluid.

7.2.1 Set up

The internal geometry of the landform is defined by disks of the same radius disposed with an arrangement that provides the maximum packaging. The geometry of the shape

is defined by the following parameters: inclination of the sides α and height h. The disks are geometrically defined by its radii and the mechanical parameters: density ρ_s, friction coefficient μ (or friction angle ϕ). No cohesion is considered. Radii, the friction and inclination angles define the global stability of the landform. In order to reach stability, the friction angle ϕ has been chosen to be greater than the inclination α.

7.2.2 Results

Following the same procedure explained in the previous simulation the numerical relationship $Re^\star - \tau^\star$ that forces the general motion of the particles is obtained. According to several papers the initiation of motion is reached when the particles fluid is greater than a given quantity, see [8], that is equal to an equivalent number of particles dependent of the particle radius. This relationship shown in Figs. 7.2.2 for several inclinations α, showing a similar relationship to Shields diagram. The results are higher than the previous since the inclination α makes difficult the motion of the particles upwards due to the inclined component of the weight. Additionally, the numerical results show that $\tau^\star$ are always greater than the experimental since the latter are measured over a flat surface. $\tau^\star$ grows with α since as ϕ increases it is more difficult to move the particle upstream. Inclination α must be always lower than ϕ to prevent the collapse of the assembly. For larger radii particles, the numerical data highly differ from Shields since the geometry of the sides is quite rough that makes the motion difficult. This phenomenon is increased with α.

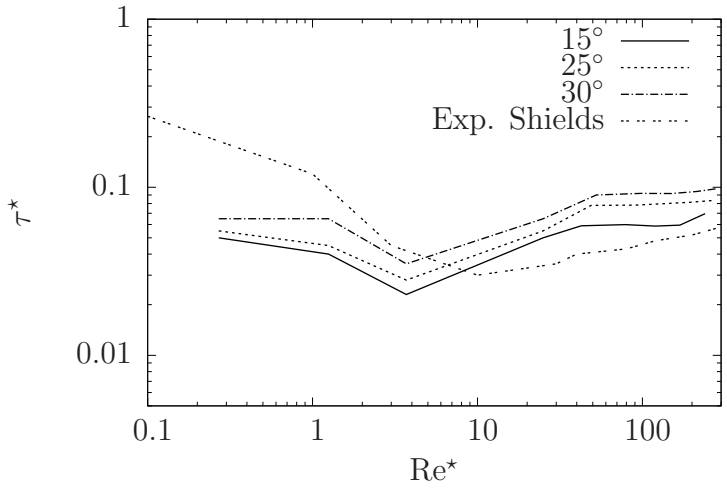

Figure 6: $Re^\star - \tau^\star$ relationship for multiple inclinations α. Comparison with experimental data for flat bed from Shields

The rolling upwards is usual mechanism for the initiation of motion. Particles never roll downwards since the friction and drag forces avoid that kind of motion. The motion

usually starts on the top side of the landform since in this location the gradient of the flow velocities is high and the motion of the particles is not so restricted. Due to the high gradient on the top particles usually lift, while those situated on the bottom and middle roll, as shown in the three snapshot depicted in Figs. 7.2.2 where it is clear that the initiation of motion always starts in in the upstream side and particles climb over the existing ones.

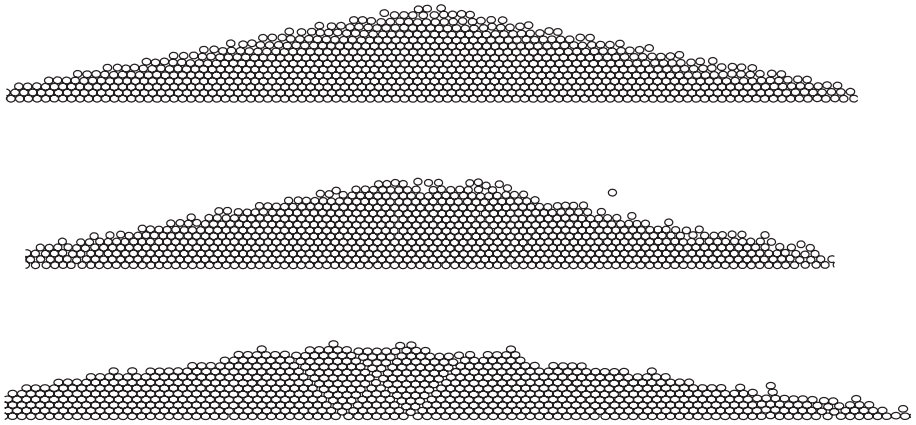

Figure 7: Snapshots at several instants in wich the initiation of motion is produced

8 CONCLUSIONS

- A coupled numerical model has been applied to simulate the initiation of motion of landforms combining DEM-FEM.

- The Discrete Element Method allows to simulate the micromechanics of the landform, therefore it provides realistic results that fit well to the experimental given by Shields. Additionally, FEM gives a good representation of the flow that acts over the landform.

- The coupled numerical method has been able to simulate accurately the experimental results and that for no experimental are available. Therefore it converts in a powerful tool to simulate the initiation of motion in complex situations where analytical results are not valid.

- It is expected to model accurately more complex problems increasing the number of particles although the parallelization will be needed.

REFERENCES

[1] R. Bravo, J. L. Pérez-Aparicio, and T. A. Laursen. An enhanced energy conserving time stepping algorithm for frictionless particle contacts. *International Journal for Numerical Methods in Engineering*, 2010.

[2] O. Gonzalez and J.C. Simo. On the stability of symplectic and energy-momentum algorithms for non-linear hamiltonian systems with symmetry. *Computer Methods in Applied Mechanics and Engineering*, 134(3-4):197–222, 1996.

[3] C. H. LING. Criteria for incipient motion of spherical sediment particles. *Journal of Hydraulic Engineering-ASCE*, 121(6):472–478, 1995.

[4] P. Ortiz, O.C. Zienkiewicz, and J. Szmelter. Hydrodynamics and transport in estuaries and rivers by the cbs finite element method. *International Journal for Numerical Methods in Engineering*, 66:1569–1586, 2006.

[5] G.H. Shi. *Discontinuous Deformation Analysis–A New Model for the Statics and Dynamics of Block Systems*. Thesis (ph.d.), University of California, Berkeley, 1988.

[6] G.H. Shi and R.E. Goodman. Two dimensional discontinuous deformation analysis. *International Journal of Analysis Methods in Geomechanics*, 9:541–556, 1985.

[7] A Shields. Application of similarity principles and turbulence research to bed-load movement. Technical report, Lab. for Hydraulic Water Resources, 1936.

[8] P.L. Wiberg and J.D. Smith. A theoretical model for saltating grains in water. *Journal of Geophysical Research*, 90:7341–7354, 1985.

[9] G. Zavarise, P. Wriggers, and U. Nackenhorst. *A Guide for Engineers to Computational Contact Mechanics*. Texts in Computational Science and Engineering. Consorzio TCN, Cagliari, 2006.

[10] O.C. Zienkiewicz, P. Nithiarasu, R. Codina, M. Vazquez, and P Ortiz. The characteristic based split procedure: An efficient the characteristic based split procedure: An efficient and accurate algorithm for fluid problems. *International Journal for Numerical Methods in Fluids*, 31(359-392), 1999.